

Scanning Tunneling Spectroscopy on the novel superconductor CaC_6

N. Bergeal, V. Dubost, Y. Noat, W. Sacks, D. Roditchev
*Institut des Nanosciences de Paris, Universités Paris 6 et 7,
UMR 7588 au CNRS, 140 rue de Lourmel 75015 Paris, France*

N. Emery, C. Hérold, J-F. Marêché, P. Lagrange
*Laboratoire de Chimie du Solide Minéral (UMR CNRS 7555),
Université Henri Poincaré Nancy I, B.P. 239, 54506 Vandoeuvre-lès-Nancy Cedex, France*

G. Loupiaz
*Institut de Minéralogie et de Physique des Milieux Condensés, IMPMC-UMR 7590,
Université Paris 6, 4 place Jussieu, F75252 Paris Cedex 05, France*

We present scanning tunneling microscopy and spectroscopy of the newly discovered superconductor CaC_6 . The tunneling conductance spectra, measured between 3 K and 15 K, show a clear superconducting gap in the quasiparticle density of states. The gap function extracted from the spectra is in good agreement with the conventional BCS theory with $\Delta(0) = 1.6 \pm 0.2$ meV. The possibility of gap anisotropy and two-gap superconductivity is also discussed. In a magnetic field, direct imaging of the vortices allows to deduce a coherence length in the ab plane $\xi_{ab} \simeq 33$ nm.

Interest in the superconducting properties of carbon-based compounds has been renewed by the discovery of superconductivity in CaC_6 and YbC_6 having a T_c of 11.5 K and 6.5 K respectively [1, 2]. Such values constitute an increase of nearly one order of magnitude of the T_c reported for Graphite Intercalation Compounds (GIC) at ambient pressure, the latest being $\text{KTI}_{1.5}\text{C}_4$ with a T_c of 2.7 K by Wachnik *et al.*[3]. A controversy has arisen about the origin of superconductivity in these materials. On the basis of self-consistent electron-phonon calculations, Calandra and Mauri [4] suggested a conventional BCS phonon-mediated mechanism where the C out-of-plane and the Ca in-plane vibrations couple mainly to electrons of the Ca Fermi surface. A similar approach has been used by Mazin [5] with comparable results. On the other hand, Csanyi *et al.*[6] developed an excitonic (QP) spectrum of these materials is thus of immediate interest.

The preparation of high-quality samples by Emery *et al.* [7] has been an important step in the experimental study of CaC_6 : it has allowed a proper measurement of the bulk superconducting parameters [8] as well as the measurement of the magnetic penetration depth, see Lamura *et al.*[9]. Their results give evidence for a mainly s-wave superconductivity, and a BCS weak coupled superconductor with a gap $\Delta(0) = 1.79$ and $2\Delta(0)/k_B T_c = 3.6 \pm 0.2$. However, in these measurements, the gap and the coherence length are obtained in an indirect manner. In this Letter, we report the first scanning tunneling microscopy and spectroscopy (STM/STS) measurements, as a function of temperature and magnetic field, giving directly the superconducting gap and the coherence length. Our results are in good agreement with a conventional BCS type superconductivity. An upper bound for the gap anisotropy is estimated.

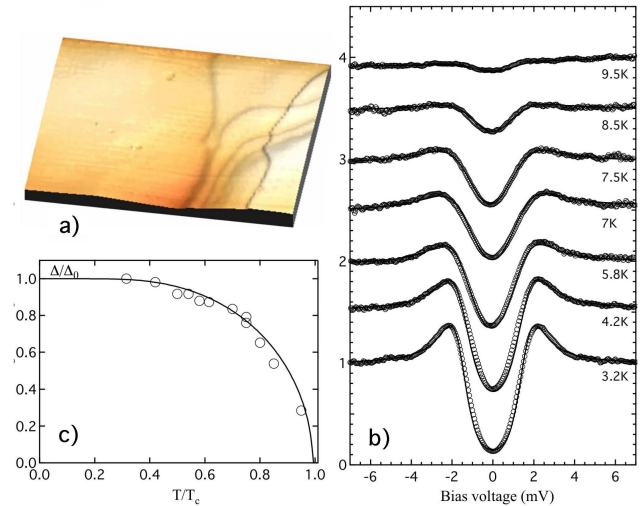


FIG. 1: (Color online) (a) Topographic image of the cleaved surface of CaC_6 ($180 \text{ nm} \times 150 \text{ nm}$). The total height difference is about 15 nm. (b) Temperature dependence of tunneling conductance spectra. Experimental data (dots) are fitted using expressions (1) and (2) with $\Gamma = 0.2$ meV. The spectra are shifted by 0.5 for clarity. (c) Temperature dependence of the superconducting energy gap extracted from b). Solid line shows the BCS $\Delta(T)$ with $T_c = 10$ K and $\Delta_0 = 1.6$ meV.

The samples were prepared by the immersion for ten days of a platelet of highly-oriented pyrolytic graphite in a molten lithium-calcium alloy at around 350°C under argon atmosphere. This procedure, described in detail in [7], leads to plate-like samples ($2 \times 2 \times 0.3$ mm in this study). They are polycrystalline with c -axis of all the crystallites parallel to each other, whereas it is disordered in the ab plane. After the synthesis, the samples, still under argon atmosphere, were embedded into sil-

ver epoxy between the STM sample holder and a cleavage screw. This method allows to prevent air-sensitive compounds from damage prior to its introduction into the UHV chamber of the microscope. The samples were cleaved under UHV, and then rapidly cooled down to 4.2 K, using a pure exchange He gas, at a pressure around 10^{-3} mBar. Further cooling to 3 K was achieved by pumping on the helium bath of the cryostat. All the measurements were carried out using freshly cut Pt/Ir tips. In the chosen tip-sample configuration, tunneling is parallel to the *c*-axis.

A typical STM topographic image is displayed figure 1(a). One can find relatively flat regions, but the terraces are not as large as those usually encountered on precursor graphite samples. Also, it appears that the material does not cleave well. This illustrates that, despite the layered structure, CaC_6 is less anisotropic than most of the other GIC and has more pronounced 3-dimensional character, in agreement with Calandra *et al.* [4]. This is also confirmed by the coherence length reported by Emery *et al.*[8] and by our measurement below.

To obtain the conductance curves in the STS configuration, symmetrical bias voltage sweeps, typically in the range ± 15 mV, were applied while acquiring the tunneling current $I(V)$. In a single measurement, 256 voltage sweeps are applied to the junction (with feedback loop open) and the corresponding current-voltage spectra are averaged in order to eliminate the major part of the noise. The dynamical conductance curve $dI/dV(V)$ is then the direct numerical derivative, without further data treatment. As is well known, at zero temperature, $dI/dV(V)$ is directly proportional to the sample QP density of states (DOS), $N_S(E_F + eV)$. Taking into account thermal broadening leads to the expression:

$$\frac{dI(V)}{dV} \propto \int_{-\infty}^{\infty} dE N_S(E) \left(-\frac{\partial f(E - eV)}{\partial V} \right) \quad (1)$$

where,

$$N_S(E) = N_n(E_F) \text{Re} \frac{E - i\Gamma}{\sqrt{(E - i\Gamma)^2 - \Delta(T)^2}} \quad (2)$$

Here $f(E)$ is the Fermi function, $N_n(E_F)$ is the normal DOS and Γ , in the BCS extended DOS, takes into account the finite QP lifetime [10]. In these expressions, any Fermi surface or gap anisotropies are not taken into account.

We performed tunneling spectroscopy in the temperature range from 3.2K to 15K. The evolution of the conductance as a function of temperature is shown in figure 1(b). The overall shape of the spectra agrees well with the extended BCS density of states (2). The set of curves can be fitted using a single isotropic gap $\Delta(T)$ and the temperature T as independant parameters, and Γ fixed at 0.2 meV in all the fits. The gap $\Delta(T)$ obtained from the fitting procedure is in good agreement with a conventional BCS self-consistent gap (figure 1 c), providing

a zero-temperature gap value $\Delta(0)$ of 1.6 ± 0.2 meV and a T_c of 10 ± 1 K. This gives a BCS ratio $2\Delta(0)/k_B T_c$ of 3.66, slightly higher than the expected value in the weak-coupling limit. T_c and $\Delta(0)$ values are close to, but slightly smaller than, those previously reported: $T_c=11.5$ K by magnetization measurements and $\Delta(0)=1.79$ meV obtained from magnetic penetration depth. The small discrepancy observed may originate from a little Ca depletion at the surface of the sample.

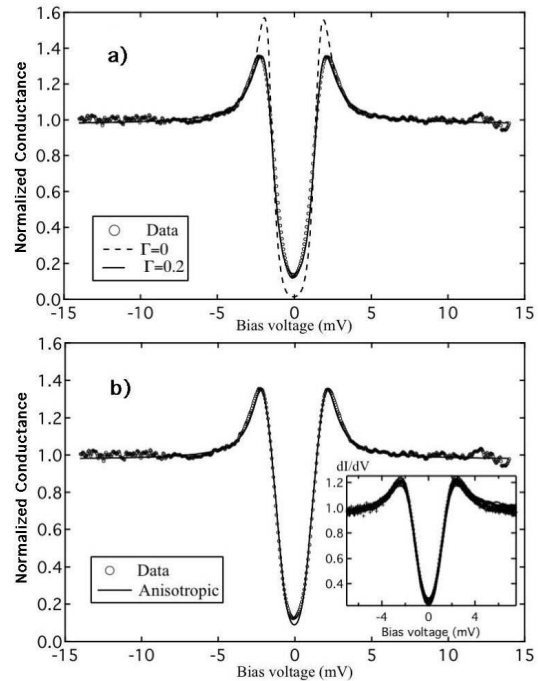


FIG. 2: (a) Effect of the parameter Γ on the conductance spectrum. Dots : experimental data at 3.2 K, dashed line: BCS fit with $\Gamma=0$, solid line: BCS fit with $\Gamma=0.2$ meV. (b) Dots : experimental data, solid line: BCS fit with a cosine dependent anisotropic gap $\Delta=1.45 \pm 0.55$ meV. Inset: conductance spectra for different tunneling resistances (11 superposed spectra from 0.1 $M\Omega$ to 10 $M\Omega$).

We now turn to a finer analysis of the tunneling spectra. In figure 2(a) we plot a typical $dI/dV(V)$ experimental spectrum and two fits obtained by considering only a single isotropic BCS gap, at the temperature $T = 3.2$ K of the junction. The first fit, with Γ set to zero, does not agree with the experimental data whereas the second fit with $\Gamma = 0.2$ meV is a perfect match. The need for this phenomenological smearing term, found often in the literature, raises the question of the real underlying physical phenomena. The Γ term was first suggested by Dynes [10], to take into account a finite QP lifetime (or imaginary part of the self-energy). However, in a STM experiment the broadening can be due to various effects: the finite QP lifetime corresponding to inelastic processes, the electronic noise of the STS, in particular a voltage jitter, and finally the anisotropy of the electronic

structure, intrinsic to the material. For conventional superconductors, even strong coupling, the QP self-energy broadening is expected to be negligible. So, the use of a Γ parameter accounts for the smearing due to the intrinsic anisotropy, and extrinsic experimental resolution, which must be distinguished. At least, a part of the Γ value is due to the resolution function of our experimental set-up.

The possibility of gap anisotropy in this material is important to consider: the GIC's were believed to be an example of two-gap superconductivity [11]. This is due to the fact that the Fermi level is crossing both the graphene π band, with a Fermi surface nearly cylindrical along the c^* axis, and the intercalate s -band, with a Fermi surface almost spherical around the central Γ point of the Brillouin zone. However, if the superconductor is anisotropic, then the tunneling geometry becomes important and one must express the precise tunneling of the sample QP, of wave vector $\vec{k} = (k_{\parallel}, k_{\perp})$ and gap parameter $\Delta_{\vec{k}}$, to the tunneling tip, or the converse.

Using the theory of Tersoff and Hamann [12], $N_S(E)$ in (1) must be replaced by the local tunneling DOS:

$$N_T(E, z) = \frac{1}{4\pi^3} \int_{\Sigma_F} dS_{\vec{k}_F} \frac{1}{|\nabla \varepsilon_{\vec{k}_F}|} T_{\vec{k}_F}(E_F, z) \frac{E}{\sqrt{E^2 - \Delta_{\vec{k}}^2}} \quad (3)$$

where the integral is over the Fermi surface Σ_F and the transmission factor is [13]:

$$T_{\vec{k}}(E, z) = |c_{\vec{k}}(E)|^2 e^{-2\alpha_k z} \quad (4)$$

In (3), ε_k is the normal spectrum, $c_{\vec{k}}$ is the amplitude of the Bloch function at the surface of the sample, and α_k is the vacuum attenuation coefficient: $\alpha_k = \sqrt{k_{\parallel}^2 + \frac{2m\varphi}{\hbar^2}}$, φ being the work function. Consequently, the main contribution to the tunneling conductance is due to states with small k_{\parallel} , or the surface Brillouin zone center (\vec{k} -selection of the barrier). Neglecting the \vec{k} -dependence of $T_{\vec{k}}(E_F, z)$ and taking a constant gap, gives back equation (2). The above equation (3) thus compactly represents the effects of Fermi surface, tunneling matrix element and gap anisotropies. In the case of c -axis tunneling, the main contribution comes essentially from states of the spherical Fermi surface of the intercalant s -band. The inset of figure 2(b) presents the conductance spectra for different tunneling resistance, i.e. for different tip-sample distances. The spectra appear unmodified, providing evidence for the minor role of the $e^{-2\alpha_k z}$ term. In the case of a two-gap superconductor, one can observe additional signatures in the conductance. This can be understood by separating the integral (3) into different Fermi surface parts. Some of the contributions can be weak, if they are linked to Fermi surface points with larger k_{\parallel} . This situation is observed in MgB₂ c -axis oriented thin films, the small gap Δ_{π} dominates the spectrum but the QP peaks are also slightly affected. No double-gapped spectra, nor extra features, have been observed on CaC₆.

Since the precise value of (3) depends on the detailed band structure, in order to estimate a possible anisotropy we adopt a gap distribution of the form:

$$\Delta(\theta) = \Delta_0 + \Delta_1 \cos(2\theta) \quad (5)$$

In this case, conductance (1) contains an additional integration over the θ parameter. The figure 2(b) displays a characteristic spectrum taken at 3.2 K and the fit with an anisotropic, cosine dependant gap with parameters $\Delta_0=1.45$ meV and $\Delta_1=0.55$ meV. However, such a strong anisotropy is not supported by the fact that the spectra are unmodified with the different tip-sample distances (inset fig 2b). Consequently, even if the occurrence of a strong anisotropy in CaC₆ or double-gap superconductivity cannot be completely excluded, it seems to be unlikely. Nevertheless, a definitive answer would require tunneling along the ab direction. Such a measurement appears difficult, given the small thickness of the samples, and the air-sensitiveness of this compound, forbidding the *ex-situ* preparation of an inverted junction, as was previously used on MgB₂ [14]. It can also be reached with a very high energy resolution. This would require very low temperatures or the use of a superconducting tip, as in the experiment of Rodrigo and Vieira [15] showing the multi-band superconductivity in NbSe₂.

We now focus on scanning tunneling spectroscopy in the presence of a magnetic field. In a ideal type II superconductor, an applied magnetic field B_a penetrates the sample in the form of vortices, each carrying one flux quantum Φ_0 . Due to energy considerations, vortices arrange in a periodic lattice, usually triangular with a spacing $d = (2\sqrt{3}\Phi_0/B_a)^{1/2}$. Each vortex is surrounded by screening currents which decay over the magnetic penetration length λ and has a core extending over the coherence length ξ , where superconductivity is suppressed. Finally, when the thermodynamic critical field H_{c2} is reached, the vortices overlap and the sample return to normal state, with a metal-like QP DOS.

In order to determine ξ , we have attempted to image the vortices by scanning tunnelling spectroscopy under a magnetic field applied perpendicular to the sample, thus to its c -axis. This configuration enables to determine only the in-plane coherence length ξ_{ab} , for the reasons of selective tunneling discussed earlier. As also mentioned, the samples do not cleave very well, and it has been difficult to obtained surfaces suitable for scanning spectroscopy. Several attempts were necessary in order to image the vortices, which appear clearly only in limited regions. The inset of figure 3 a) displays the normalized zero bias conductance map, obtained for a magnetic field $B_a=0.05$ T where bright colors correspond to vortex cores and dark colors to superconducting areas. For this value of B_a , the inter-vortex distance is of the same order than the magnetic penetration depth λ [9]. In this case, the screening currents are expected to affect the QP DOS in the superconducting region between the vortices. This

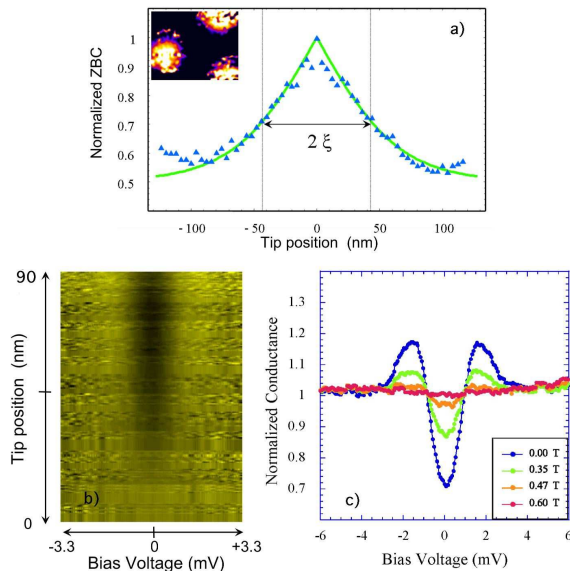


FIG. 3: (Color online) (a) Normalized zero bias conductance versus position from the vortex center. Inset: Zero-bias conductance map showing three vortices (170 nm×230 nm). (b) Evolution of the $dI/dV(V)$ spectra on a grey scale as a function of the distance to the vortex core. (c) Normalized conductance spectra with increasing magnetic field at $T=5.5\text{K}$.

can be seen in the figure 3(b) which displays the evolution of the $dI/dV(V)$ spectra on a grey scale as one goes from the inter-vortex space to the core. Outside the core, the zero bias conductance is significant and the QP peaks are affected. A normalized zero bias vortex profile is shown in figure 3(a). Following reference [19], the zero bias profile can be fitted by the formula below, derived from the Ginzburg-Landau expression for the superconducting order parameter :

$$\sigma(r, 0) = \sigma_0 + (1 - \sigma_0) \times (1 - \tanh(r/(\sqrt{2}\xi))) \quad (6)$$

where σ_0 is the normalized zero bias conductance away from a vortex core and r the distance to the vortex center. The fit yields a coherence length of $\xi_{ab}=46\text{ nm}$ at $T=5.5\text{K}$ and an extrapolated $\xi_{ab}(0)=33\text{ nm}$ at zero temperature. This value is in a good agreement with $\xi_{ab}(0)=35\text{ nm}$ reported from bulk magnetic measurements [8].

In the case of a clean superconductor, Andreev bound states [16] due to the confinement of QPs inside the vortex core are expected to appear as a zero bias conductance peak in the tunneling conductance [17]. However, in the dirty limit, the scattering of these states results in a smearing of the peaks to bumps and, eventually, to a flat metal-like DOS. This has been previously observed by STS measurement in $\text{Nb}_{1-x}\text{Ta}_x\text{Se}_2$ at 1.3 K [18]. Even if some of our spectra display some weak sub-gap features close to the zero bias, similar to those of reference [18], there is no clear evidence for the presence of bound

states. This is consistent with the fact that these samples are in the dirty limit, in accordance with ref [9]. The figure 3(b) displays the evolution of conductance spectra at 5.5K with further increase of magnetic field. The main effect is to smear the QP peaks and to fill the gap progressively with QP states. For a field $B_a \simeq 0.6\text{ T}$, the conductance displays a normal DOS indicating that the sample has returned to the normal state. This value is larger than the one extracted both from magnetometry measurement and from the value of ξ deduced above. In this “zero-field cooled” experiment, this is likely due to flux trapped in some poorer quality area of the sample which modifies locally the magnetic field distribution.

In conclusion, we have performed tunneling spectroscopy measurements on the superconducting Ca intercalated graphite, CaC_6 , at various temperatures. The spectra and their temperature dependence are consistent with a single isotropic BCS gap of 1.6 meV, with no clear indication for additional contribution. Nevertheless, further measurements in different tip-sample configurations (a-axis for instance) will be necessary to give a definitive conclusion concerning the possibility of two-gap superconductivity or strong gap anisotropy. In the presence of a low magnetic field, the coherence length $\xi_{ab} = 33\text{ nm}$ is extracted directly from the real space vortex imaging.

This work was supported by project GPB *Matériaux aux propriétés remarquables*.

-
- [1] T. E. Weller et al., Nature Physics **1**, 39-41 (2005).
 - [2] Of historical interest, CaC_6 was first prepared in 1980 (D. Guerard, M. Chaabouni, P. Lagrange, M. El Makrini and A. Herold, Carbon **18** 257-264 (1980)). Just like MgB_2 , CaC_6 is “an old material but a new superconductor”.
 - [3] R. A. Wachnik et al., Solid state commun. **43**, 5-8 (1982).
 - [4] M. Calandra, F. Mauri Phys. Rev. Lett. **95**, 237002 (2005).
 - [5] I. I. Mazin Phys. Rev. Lett. **95**, 227001 (2005).
 - [6] G. Csanyi et al., Nature Physics **1**, 42-45 (2005).
 - [7] N. Emery, C. Herold, Ph. Lagrange, J. Solid State Chem. **178**, 2947-2952 (2005).
 - [8] N. Emery et al., Phys. Rev. Lett. **95**, 087003 (2005).
 - [9] G. Lamura et al., Phys. Rev. Lett. **96**, 107008 (2006).
 - [10] R. C. Dynes, V. Narayanamurti and J. P. Garno Phys. Rev. Lett. **41**, 1509 (1978).
 - [11] R. Al-Jishi, Phys. Rev. B **28**, 112-116 (1983).
 - [12] J. Tersoff D. R. Hammam Phys. Rev. Lett. **50**, 1998 (1983).
 - [13] Higher Bloch terms have been neglected.
 - [14] F. Giubileo et al., Phys. Rev. Lett. **62**, 177008 (2001).
 - [15] J. G. Rodrigo, S. Vieira, Physica C **404**, 306, (2004).
 - [16] C. Caroli, P. G. De Gennes, J. Matricon Phys. Lett. **9**, 307 (1964).
 - [17] H. F. Hess et al. Phys. Rev. Lett. **62**, 214 (1989).
 - [18] Ch. Renner et al., Phys. Rev Lett. **67**, 1650 (1991)
 - [19] M. R. Eskildsen et al. Phys. Rev. Lett. **89**, 187003 (2002)